Vacuum 188 (2021) 110200

Contents lists available at ScienceDirect

Vacuum

journal homepage: http://www.elsevier.com/locate/vacuum

Characterization of Ti–Zr–V thin films deposited by DC and unipolar pulsed DC magnetron sputtering

Sihui Wang [a], Wei Wei [a,*], Yonghao Gao [b], Haibin Pan [a], Yong Wang [a,**]

[a] National Synchrotron Radiation Laboratory, University of Science and Technology of China, HeFei, 230029, PR China
[b] School of Materials Science and Engineering, Central South University, Changsha, 410083, PR China

ARTICLE INFO

Keywords:
Magnetron sputtering
Ti–Zr–V
Non-evaporable getter films
XPS
Annealing treatment

ABSTRACT

Ternary Ti–Zr–V getter films with approximately equal atomic concentrations were deposited on oxygen free copper substrates by magnetron sputtering using DC and unipolar pulsed DC current modes. The thin film morphologies were studied using scanning electron microscopy, atomic force microscopy, while their chemical and phase compositions were investigated by energy dispersive spectroscopy and X-ray diffraction, respectively. The chemical states within the superficial regions of the films were characterized by X-ray photoelectron spectroscopy in ultra-high vacuum. The results indicate that both current modes promote formation of porous thin films, while the microstructure of the DC film is much finer than that of the unipolar pulsed DC film. Initially, the thin films were covered by oxides of Ti, Zr and V that are reduced upon annealing treatment; those within the DC film present faster reduction kinetics as compared with that of the unipolar pulsed DC film.

1. Introduction

Operation of advanced particle accelerators has long been challenged by the presence of residual gases that sacrifice beam stabilities and lifetime [1–4]. Simply increasing the number of external pumps to evacuate the residual gases is impractical due to space limitations in the small-aperture vacuum chambers of modern compacted accelerators [5]. Therefore, various methods have been proposed to solve such problems, of which coating the vacuum chamber with non-evaporable getter (NEG) films is considered the most effective [6–11].

The basic principle of NEG relies on the surface absorption of gas molecules and their subsequent diffusion into the bulk material [12]. Therefore, the desirable NEG materials should satisfy such demands as high solubility and sufficient diffusivity of absorbed residual gas molecular. In this regard, an outstanding NEG thin film comprising Ti, Zr and V were invented in the European Organization for Nuclear Research (CERN) in 1998 [13] and now has been widely utilized in the advanced accelerators [14–18], of which Ti and Zr possess high solubility of oxygen (the most common residual gas in the vacuum chamber), while V increases the inwards diffusion rate of oxygen [19,20].

Chemical compositions of the films have been altered using different types of cathode target. Three targets made of pure Ti, Zr and V metals were used by Benvenuti et al. [21] and Prodromides et al. [22], and the film composition was controlled by applying different power to each target. Inter-twisted pure metal wires were used for production of films on the inner wall of vacuum tubes [13]. The heterogeneous chemical distribution is inevitable by using such target configurations, such drawbacks can be eliminated by using ternary Ti–Zr–V alloy as the sputtering cathode [19,23,24].

Apart from chemical composition, film structure imposes significant effects. It has been shown that increased surface roughness can enhance the pumping efficiency by increasing the density of the effective absorption sites in NEG films [21]. Refining the microstructure is also beneficial for the vacuum properties as the grain boundaries provides additional inwards diffusion path for adsorbed atoms [6,25]. Pores within the thin films not only provide additional diffusion paths but also increase the effective surface area, which is considered beneficial for NEG films [26]. The alignment of grains in the films also plays a part; it has been reported that columnar grains grown in Zone I of the Thornton model [27] are better in terms of pumping properties as relatively straight boundaries between the neighboring grains reduce the corresponding diffusion length [12].

The microstructure of Ti–Zr–V thin films is affected by various sputtering parameters, such as substrate temperature, chamber pressure,

* Corresponding author.
** Corresponding author.
E-mail addresses: platowei@ustc.edu.cn (W. Wei), ywang@ustc.edu.cn (Y. Wang).

https://doi.org/10.1016/j.vacuum.2021.110200
Received 2 November 2020; Received in revised form 7 March 2021; Accepted 10 March 2021
Available online 15 March 2021

sputtering gas, magnetron power and current modes, etc. These sputtering parameters are normally non-linearly correlated, increasing complexity in manipulating resulting film characteristics. Tremendous effort has been devoted to this area, and some widely accepted insights have been achieved. Substrate temperature is usually altered deliberately to influence the lateral movement of the sputtered atoms deposited on the substrate surface, thus affecting the roughness, porosity and grain texture of the final film [27,28]. The base pressure in the chamber prior to deposition should be sufficiently low, otherwise the chemical purity of resulting films might be compromised [29]. Different sputtering yields might be achieved by varying sputtering gases with different atomic numbers [30]. Applied current modes also affect growth mechanisms of the films, thus influencing their characteristics. Different current modes, including DC, plused DC [25,31] and radio frequency (RF) [32], has been utilized in preparing NEG thin films. Malyshev et al. [31] reported that DC current will promote the formation of columnar structures, while dense structures are produced by pulsed DC sputtering. However, porous and columnar (rather than dense) structures have also been produced by pulsed DC current [23]. Despite this current mode being widely used in reactive magnetron sputtering (as Ti–Zr–V film sputtering is a non-reactive process), the data on the effects of pulsed DC on the resulting film characteristics is still very limited, and the question as to how the thin films are affected by the magnetron sputtering process is still open for discussion.

In the present work, Ti–Zr–V thin films were deposited by magnetron sputtering under DC and unipolar pulsed DC current modes. Characteristics of produced films were comparatively studied, and the chemical state evolution in the superficial region of the films during thermal treatment at various temperatures was evaluated using X-ray photoelectron spectroscopy (XPS) technique.

2. Experimental procedures

Magnetron sputtering is used to produce Ti–Zr–V thin films on oxygen free copper (OFC) substrates. Before deposition the OFC substrates were ultrasonically cleaned by dipping in an alkaline solution and subsequently in an acid solution (RSB-117, *Jiangxi RuisiBo New Material Co., Ltd.*) to remove the surface corrosion products. A ternary Ti–Zr–V alloy rod with a diameter of 3 mm with equal atomic ratios of the elements was used as the target. Since increased fraction of grain boundaries and surface roughness are proven beneficial for vacuum properties of the NEG films, no pre-heating was conducted on the substrate to promote the formation of refined grains (to increase grain boundary volumes) as well as to yield rough films [16]. The thin films were deposited using either DC or unipolar pulsed DC current mode. The applied current was kept constant at 0.1 A for DC mode. In the unipolar pulsed DC mode, the rectangular waveforms were utilized, the peak current was set at 0.1 A, the duty cycle of the pulsed waveform was 38.5%, and the corresponding frequency was 50 kHz. The magnetic field strength used for the deposition was 170 G, and the background base pressure in the deposition chamber before sputtering was 5×10^{-5} Pa. The sputtering gas used in the present study was Kr due to its high sputtering yield, and the working pressure was 1 Pa.

The surface and cross-sectional morphologies of the thin films were characterized using Tescan MAIA3 Schottky field emission scanning electron microscope (SEM) equipped with Oxford Instruments X-Max 50 energy dispersive spectroscopy (EDS) attachment for chemical analysis. The through-thickness fracture topography of the thin films was obtained by bending the deposited samples to evaluate the texture of the grains. X-ray diffraction (XRD) was applied to characterize the phase composition of the sputtered films using a Rigaku SmartLab X-ray diffractometer operated with Cu Kα radiation ($\lambda = 0.154$ nm). The samples were scanned under the Bragg Brentano (θ-2θ) geometry in the 2θ range of 30° to 70°, with a step size of 0.02° and a scan rate of 3 deg/min. The obtained diffraction patterns were analyzed using MDI JADE software. The film surface roughness was evaluated using a DI Innova scanning probe microscope operated in both non-contact tapping and phase mode under ambient conditions.

X-ray photoelectron spectroscopy characterization is performed with a VG-ScientaR3000 hemispherical analyzer using non-monochromatic Mg Kα radiation (1253.6 eV) as excitation source to identify the evolution of chemical states within the top surface of the thin films while being annealed at different temperatures. Prior to XPS acquisition, the Ti–Zr–V thin films were not sputtered by any high-energy beams to prevent any possible damages by the bombardment. The base pressure during spectra acquisition was better than 2×10^{-10} Torr, and the XPS data was acquired from a surface area of 800×1000 μm^2. XPS data was collected step by step from the same sample after annealing for 1 h at pre-set temperatures. High-resolution spectra were collected using an energy step of 0.05 eV. The C1s, Ti 2p and Zr 3d orbitals were individually collected within their respective binding energy ranges, i.e., 280–290 eV, 468-452 eV and 178–186 eV, respectively, while that for the V 2p and O 1s regions were collected together in the binding energy ranging from 509 to 538 eV. The conventional method referencing the binding energy scale with the binding energy (BE) of C 1s signals was carefully applied in the present study to avoid misinterpreting the XPS results due to the uncertainties in the BE of the C 1s peaks [33]. Considering the sum of the BE of the C 1s signal and the corresponding work function of the sample is "constant at 289.5 ± 0.15 eV, irrespective of materials system and air exposure time" [34], the sample work function Φ_s was measured first, and then the true value of BE for the C 1s peaks was easily calculated as 289.5-Φ_s. Φ_s was measured by applying a bias of −10 V to the sample while being excited by a photon beam of 170 eV. Following the method described in Ref. [35], Φ_s was determined to be 5 eV. Therefore, the binding energy scale in the presented study was referenced against the true BE (284.5 eV) of the C 1s peak.

The XPS spectrum was deconvoluted using CasaXPS software. Before modelling, Shirley background has been subtracted for all spectra. The correlation between the doublets associated with the p- and d-orbital splitting were strictly constrained. The 1:2 and 2:3 ratios of peak intensities of $2p_{1/2}$:$2p_{3/2}$ and $3d_{3/2}$:$3d_{5/2}$ doublets were applied. The constrains to the corresponding separation energy and the characteristic binding energy of each orbital peak, depending on the valence states, were selected from NIST Database and X-ray photoelectron spectroscopy handbook [36]. The symmetrical peaks from oxidized states were fitted using Gaussian (70%)-Lorentzian (30%) profile, while the asymmetrical peaks associated with the metallic state were modelled using LA function defined in CasaXPS software. The intensities of the resolved peaks were used to calculate the fractions of corresponding chemical states.

3. Results and discussion

3.1. Surface morphology characterization

Surface morphologies of the Ti–Zr–V thin films deposited in the present study (Fig. 1) exhibit highly porous characteristics, with porosity and dimensions of the pores being highly dependent on the applied current mode. The DC current results in a much coarser porous morphology as compared with the pulsed DC mode. The diameter of the pores in the films are distributed in the range of 0.2–5.0 μm. It is clear that the large pores are actually comprised of several smaller pores, leaving large openings at the top. The surface porosity of DC films is about 3.5%, while that for the pulsed DC films is around 10%. It seems that the thin films actually comprise an aggregate of clusters, whose appearance and size are heavily affected by the applied current mode. Under DC current mode, the average size of the clusters is about 90 nm, while those of the pulsed DC film is considerably larger, 6 μm. The surface roughness of the two films was evaluated using AFM with a scanning area of 5 μm × 5 μm, and the results are presented in Fig. 2. The films produced using the DC current possess a mean surface roughness of 64.8 nm, while it is 20.8 nm for the film produced using the unipolar pulsed DC mode.

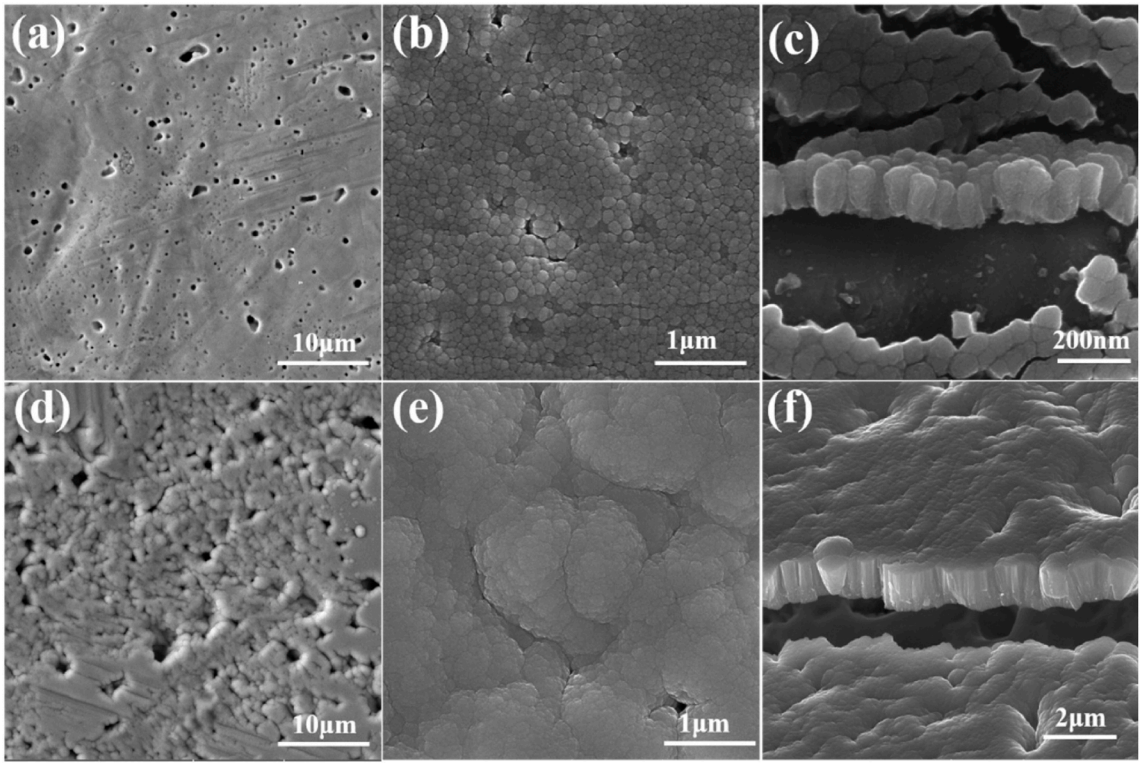

Fig. 1. Surface morphology of Ti–Zr–V films sputtered with various current modes (a)~(c) DC and (d)~(f) Unipolar Pulsed DC.

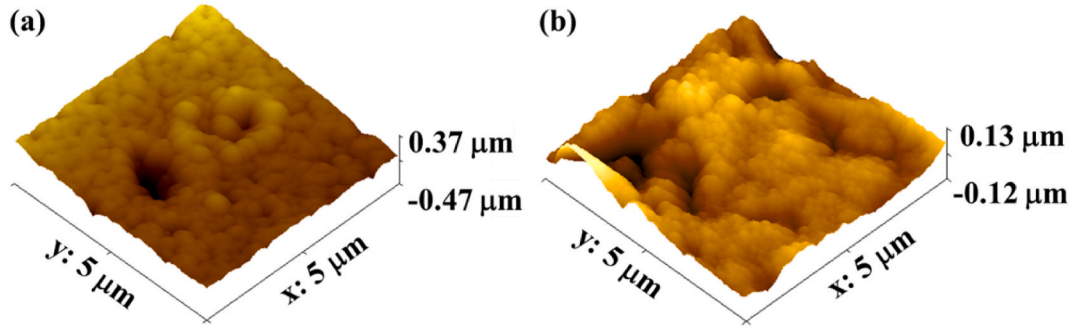

Fig. 2. Three-D AFM surface topography of the Ti–Zr–V getter films deposited using (a) DC and (b) unipolar pulsed DC current mode.

The cross-sectional images of the two films present different characteristics (Fig. 1). Typical columnar growth of the thin films is observed in both scenarios, according to Fig. 1 (c) and (f). Such growth mechanism is more visible by depositing the thin films on silicon wafer using the same sputtering parameters (the results not shown here), as it is much easier to get the cross-sectional fracture topography on Si substrate. It should be mentioned that the thickness of the thin films cannot be derived reliably from the cross-sectional images shown in Fig. 1 because the film suffered from severe plastic deformation and wear damage during bending to expose the fracture topography.

The chemical compositions of the two films were characterized using EDX analysis, and roughly equal atomic concentrations of 33.2Ti-34.4Zr-32.4V and 32.9Ti-36.2Zr-30.9V (at.%) were derived from the DC- and pulsed DC- films, respectively.

The X-ray diffraction patterns of the films sputtered with various current modes are presented in Fig. 3. The strong peaks at $2\theta = 43.5^{\circ}$ and 50.5° are associated with the (111) and (200) planes of the substrate copper. The peaks diffracted by the Ti–Zr–V films are significantly weaker compared to those from the Cu substrate because the thickness of the films is rather low. However, when zoomed in, three peaks at $2\theta =$

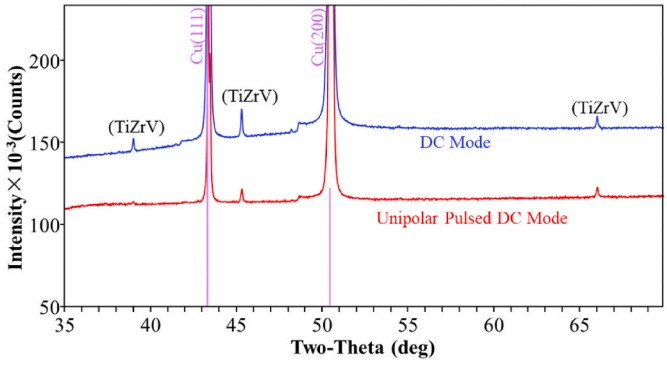

Fig. 3. XRD analysis of the Ti–Zr–V films sputtered with different current modes. The solid green lines indicate the standard powder diffraction pattern of FCC-Ti, while their closest dashed lines mark the 2-theta positions (and the peak shift) of our experimental results.

39.0°, 45.3° and 66.0° can still be distinguished. Such peaks are attributed to the Ti–Zr–V thin film. Even though it is reported that the magnetron sputtering normally yield a mixture of amorphous phases and crystallites, the thin films in the present study are well crystallized as only sharp peaks are identified in Fig. 3. Unlike the single peak around $2\theta = 35\text{-}40°$ normally reported for the Ti–Zr–V thin film in the existing literature [22,28], additional two peaks at $2\theta = 45.3°$ and 66.0° are also identified. No more peaks can be diffracted even though the scanning 2-theta range was extended beyond 120°. The number of the peaks are not sufficient to determine neither the phase compositions nor the corresponding crystallographic structures. It is also not sufficient to tell whether the three peaks are diffracted from a single phase or from a mixture of several phases, therefore, they are assigned as (TiZrV) in Fig. 3 following those published in the literature [22,28].

3.2. Chemical state evaluation by XPS

The evolution of the valence states on the superficial surface of the DC and unipolar pulsed DC films subjected to annealing at different temperatures was evaluated by XPS, and the results are presented in Fig. 4 and Fig. 5, respectively. As for the DC film (Fig. 4), apparent shifts in the XPS peaks of Ti 2p, Zr 3d and O 1s + V 2p are identified while increasing the annealing temperature, and the symmetries of the XPS peaks also evolve dramatically. Specifically, two symmetrical XPS peaks are detected at 458.6 eV and 464.2 eV with a separation energy of 5.6 eV as corresponding to the Ti $2p_{3/2}$ and Ti $2p_{1/2}$ orbitals in the valence state of Ti(IV) [36]. Upon annealing at 150 °C, significant changes of the Ti 2p peaks involve broadening and shifting towards lower binding energy. In this case, the Ti $2p_{3/2}$ and Ti $2p_{1/2}$ peaks have shifted to 457.5 eV and 463.4 eV, respectively. Moreover, the symmetry of the peaks, especially of the Ti $2p_{3/2}$ peak, has been sacrificed with the presence of a tail on the lower binding energy side. Such characteristics indicate the formation of Ti species at lower valent states and their co-existence with Ti(IV). As the characteristic binding energy of any metallic element decreases while reducing its valence states, the lowest binding energy is normally observed from its metallic state. When the annealing temperature is increased further to 180 °C, positions of the peaks remain almost unchanged, but their widths and asymmetry of the corresponding Ti $2p_{3/2}$ peaks increase gradually, indicating the changes in the relative fraction of Ti with different oxidized states.

The 3d peaks of Zr in the DC film upon annealing are shown in Fig. 4 (b). For the as-received DC film, the two 3d peaks are sharp and intense, however, the ratio of the FWHM to the height of the peaks is increased as the annealing temperature increases. As compared with the $3d_{5/2}$ peak of Zr from the as-received DC film, this peak is shifted by 0.1 eV towards higher binding energy in the sample annealed at 150 °C. Such shift becomes very dramatic (by 0.8 eV) when the annealing temperature is increased to 160 °C, indicating the oxidation of Zr compounds. Nevertheless, the shifting direction reverses as the temperature increases further through 170 °C–180 °C, suggesting the reduction of Zr oxides. Similar to the Ti 2p peaks, the symmetry of the Zr 3d peaks are also compromised as the DC film is annealed at 180 °C.

The shift of V $2p_{3/2}$ peaks with increasing temperature is much more significant, from 515 eV of the as-received DC film to 512 eV of the 180 °C annealed DC film. On the other hand, the V $2p_{3/2}$ peak of the as-received DC film is relatively steep and sharp as compared with its thermally annealed counterparts. With increasing annealing temperature, the V $2p_{3/2}$ peaks tend to spread due to the co-existence of various chemical states of vanadium.

The XPS spectra of the unipolar pulsed DC film during thermal treatment is presented in Fig. 5. Compared with that of DC film, positions of Ti 2p and Zr 3d peaks remain almost unchanged, but the shift of V $2p_{3/2}$ peak towards lower binding energies is still apparent. In addition, appreciable evolution of the shape of Ti 2p, Zr 3d and V 2p peaks was identified after thermal treatment. Specifically, the symmetry of peaks (Ti $2p_{3/2}$ and V $2p_{3/2}$) is reduced, and the dragging tail becomes apparent. Moreover, similar to that of the DC film, spreading of V $2p_{3/2}$ peak (around 525 eV) upon annealing is also observed in the unipolar pulsed DC film. Such facts indicate that the thermal exposure induces chemical state evolution of Ti, Zr and V elements, and such evolution is much more significant for vanadium.

Apart from the presence of Ti, Zr and V, appreciable amount of O and C are also identified in both films from the XPS analysis, as shown by the O1s (Figs. 4 (c) and Fig. 5(c)) and C 1s (Figs. 4 (d) and Fig. 5(d)) peaks. The C content originates from the environmental contamination when handling the samples. O is observed because of the high oxygen affinity of Ti in the thin films. During thermal annealing, the positions of the O1s and C1s peaks remain almost unchanged, but their intensities have evolved slightly. The integrated area under the O 1s peak (and above the Shirley background) has reduced by ~4.3% when the as-received DC film was heated to 180 °C, which might be attributed to the inwards diffusion of O into the bulk of the thin film, and the declining trend of O content on the surface of NEG films upon heating is consistent with that reported in Ref. [37]. The C1s peak intensity of the as-received film increases by about 11% when the sample is simply annealed at 150 °C, and the C 1s peaks reduces gradually as the annealing temperature increases, for example, by 7.9% when the annealing temperature increases from 150 °C to 180 °C.

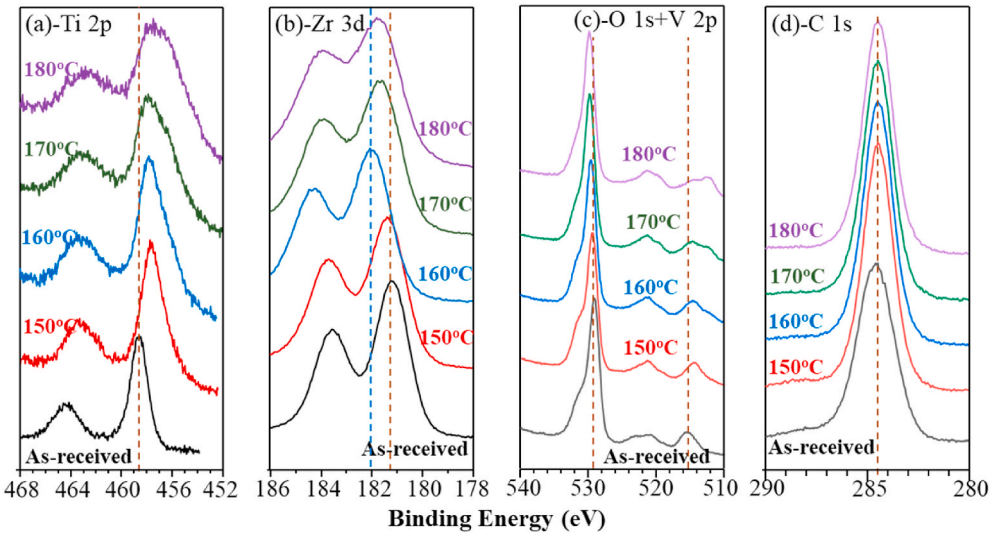

Fig. 4. Variation of XPS spectra of the DC film with increasing annealing temperatures, (a) Ti 2p, (b) Zr 3d, (c) O 1s + V 2p and (d) C 1s.

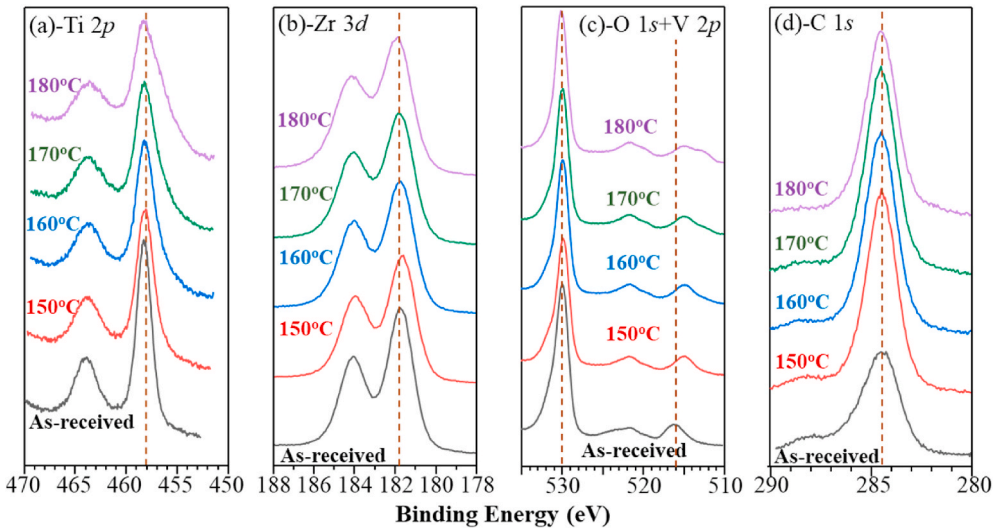

Fig. 5. Variation of XPS spectra of the Unipolar Pulsed DC film with increasing annealing temperatures, (a) Ti 2p, (b) Zr 3d, (c) O 1s + V 2p and (d) C 1s.

To quantitatively evaluate the evolution of the surface chemical states during thermal treatment, collected XPS spectra were deconvoluted and the corresponding results are presented in Fig. 6 and Fig. 7. From Fig. 6 (a) it is clear that Ti atoms in the as-received DC films are mainly in their highest oxidized state, Ti (IV). Considering the presence of a characteristic peak of O 1s at 529–530 eV (Fig. 6 (c)), it is straightforward that Ti atoms are combined with O to form TiO_2 [36]. When the sample is annealed at 150 °C, two $2p_{3/2}$ peaks with FWHM = 2.0 eV can be resolved at 457.5 and 455.4 eV, associated with Ti_2O_3 and TiO, respectively [38], suggesting TiO_2 oxides in the as-received DC film are partially reduced to lower valence states. By comparing the intensities of $2p_{3/2}$ peaks (the relative sensitivity factor (RSF) of the $2p_{3/2}$ peaks is set to be 1, while that of $2p_{1/2}$ peaks is set at 0), it is easy to conclude that the fractions of the Ti atoms in TiO_2, Ti_2O_3 and TiO are 7.28%, 78.13% and 14.59% respectively (Fig. 8(a)). When the annealing temperature is increased to 160 °C, these three oxides can still be identified, but the fraction of TiO increases to 20.35%. With further increase in temperature to 170 °C, the peaks associated with TiO_2 disappear, but a new $2p_{3/2}$ peak associated with metallic Ti (Ti^0) is identified at 453.79 eV (FHWM = 0.92 eV). The compromised symmetry of collected XPS spectra is therefore due to the distribution of unfilled one-electron level of metallic Ti^0. The co-existence of Ti_2O_3, TiO and metallic Ti^0 is also identified in the sample annealed at 180 °C (Fig. 6 (a)), but their relative fractions change significantly, with the fraction of metallic Ti^0 almost tripled to 16.06% (Fig. 8(a)).

It is evident that valence states of Zr present in the DC film also evolve upon thermal exposure after resolving the collected Zr 3d XPS spectra (Fig. 6(b)). Two characteristic $3d_{5/2}$ peaks at 182.16 eV (FWHM = 1.58 eV) and 181.16 eV (FWHM = 1.51 eV) are resolved from the as-received DC film and attributed to the presence of oxidized states of Zr (IV) and Zr(III), respectively [23]. The intensities of corresponding $3d_{5/2}$ peaks are compared after zeroing RSF of corresponding $3d_{3/2}$ doublets, the results suggests the dominance of Zr(III), 94%, in the as-received sample. Annealing the sample at 150 °C for 1 h leads to an additional $3d_{5/2}$ peak at 180.9 eV (FWHM = 2.0 eV), indicating the formation of marginal amount of Zr(II) (Fig. 8(b)). The co-existence of Zr(IV), Zr(III) and Zr(II) persists and the oxidized Zr is never reduced to its metallic state even though the annealing temperature is increased to 180 °C.

As shown in Fig. 6(c), the vanadium atoms have been oxidized to their higher oxidation states of V(IV) and V(III) in the as-received DC film, leading to the characteristic V $2p_{3/2}$ peaks at 518.78eV (FWHM = 3.2 eV) and 515.11 eV (FWHM = 3.0 eV), respectively. When the DC film is maintained at 150 °C for 1 h, V(IV) compounds vanish, accompanied with the formation of V(II) and metallic V^0, which are verified by V $2p_{3/2}$ peaks resolved at 514.00 eV (FWHM = 2.3 eV) and 512.18 eV (FWHM = 1.3 eV) respectively. Meanwhile, the fraction of V(III) increased from 44.6% in the as-received DC film to 59.0%, as shown in Fig. 8(c). About 17.4% of V has also been reduced to its metallic state V^0 at 150 °C. With further increase in the annealing temperature, the fraction of V(III) gradually declined while that of metallic V^0 increased to almost 50% at 180 °C (Fig. 8(c)).

Thermal exposure of the unipolar pulsed DC film yields the same trend regarding the chemical state evolution on the superficial coating region (Fig. 7). In the as-received unipolar pulsed DC film, Ti exists in its highest oxide state, Ti(IVIV), as supported by the resolved XPS spectra shown in Fig. 7 (a). When the film is annealed at 150 °C, a fraction of Ti (IV) reduces to its lower oxidization state Ti(III), 34.4%, and Ti(II), 4.8%. Such co-existence of the three oxidized states is retained even though the annealing temperature increases to 180 °C. However, the share of each component various gradually. Specifically, the share of the lowest sub-oxides Ti(II) increases to 17.7% at 180 °C. The most significant difference as compared to the DC film is that Ti oxides are never reduced to their metallic state Ti^0 in the unipolar pulsed DC film.

As shown in Fig. 7(b), three valence states of Zr (Zr(IV), Zr(III) and Zr (II)) have been identified after resolving the XPS spectra of the as-received unipolar pulsed DC film. Zr(III) accounts for the largest share (87.9%) as similar to that of the DC film. The difference from that of DC film lies in the presence of Zr(II) in the as-received unipolar pulsed DC film, although its fraction is marginal (3.1%). Annealing the film does not induce any significant changes to the valence states and their fractions of Zr, the dominance of Zr(III) is not challenged by its counterparts even though its share reduces to 79.1% at 180 °C.

Fitting results of the O1s + V2p spectra of the unipolar pulsed DC film is presented in Fig. 7(c). While the synthetic envelope matches reasonably well with the experimental spectra for the V $2p_{3/2}$ peaks, the V $2p_{1/2}$ peaks suffered significant under-fitting. Therefore, the quantitative analysis is only based on the V $2p_{3/2}$ peaks, which is believed to yield acceptable accuracy [38]. While all the vanadium atoms exist as V (IV) and V(III) in the as-received DC film (Fig. 6(c)), additional component of V(V) (23.0%) is also identified in the unipolar pulsed DC film as verified by the resolved V $2p_{3/2}$ peak at 517.1 eV (FWHM = 1.5 eV). When the sample is annealed at 150 °C, the valence states of vanadium evolve significantly with the disappearance of V(V) and V(IV) as well as formation of V(II) (14.2%) observed. Meanwhile, the share of V (III) increases from 43.4% in the as-received film to 85.8% following annealing at 150 °C. After increasing the annealing temperature to 160 °C, a part of V is converted to its metallic state V^0 (9.8%), while the fraction of V(II) slightly increases to 15.0% and V(III) content reduces

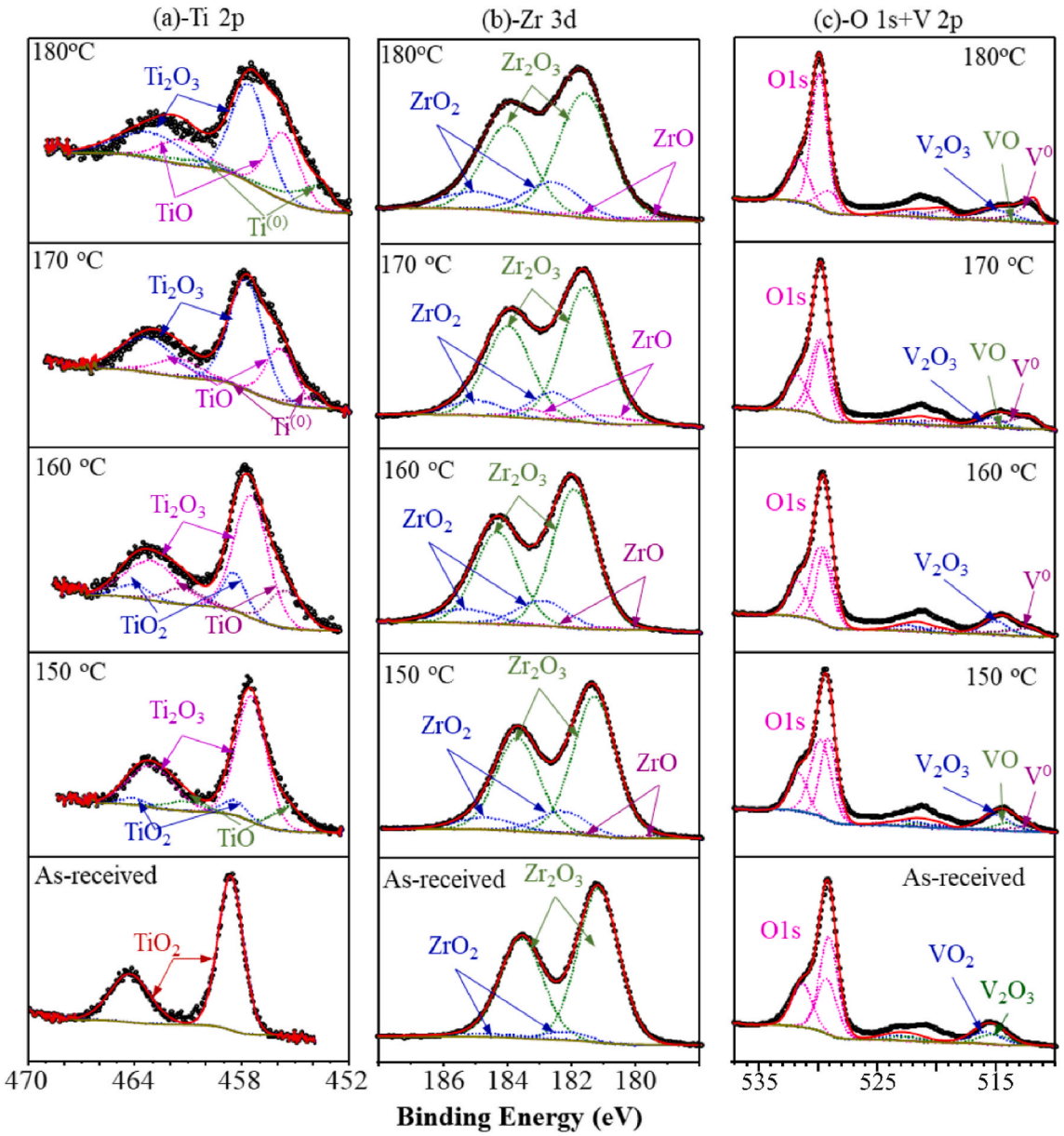

Fig. 6. Resolved XPS spectra collected from the DC film, (a) Ti 2p, (b) Zr 3d and (c) V 2p + O 1s orbitals. The line represented by the discrete circles shows the raw data, while the red line is the synthetic envelope. The dashed lines represent the individual components resolved out of the collected spectra.

considerably to 75.1%, as shown in Fig. 7(c). When the annealing temperature is further increased to 170 °C and 180 °C, the co-existence of V(III), V(II) and V^0 is retained while their relative fractions change gradually. Specifically, the share of V^0 increases, reaching 35.0% at 180 °C while the fraction of V(III) declines to 57.2%.

Fig. 8 summaries the evolution of each valence state during heat treatment with increasing temperature. The evolution trends of Ti valence states in the two films are quite similar (Fig. 8(a)). The oxidation state Ti(IV) in the as-received film declines dramatically when it is heated to 150 °C, and then reduces gradually (although with a minor fluctuation at 160 °C for DC film and at 180 °C for the unipolar pulsed DC film) at a much lower rate when the annealing temperature increases to 180 °C. Meanwhile, the amount of Ti(III) increases first before beginning to decline. The turning points are 150 °C and 160 °C for the DC and unipolar pulsed DC films, respectively. The share of Ti(II) monotonically increases for both films, and a fraction of Ti in the DC film is eventually reduced to its metallic state (Ti^0) while such reduction never happens in the unipolar pulsed DC film. Such evolution in chemical states of Ti suggests step-by-step reduction from its higher to lower oxidation states, that is Ti(IV)→Ti(III)→Ti(II)→Ti^0, which is in agreement with existing literature [39]. Therefore, dramatic reduction of Ti (IV) is associated with considerable increase in Ti(III) content, such transformation of Ti(IV) to Ti(III) does not exclude parallel processes such as reduction of Ti(III) to Ti(II).

Transitions in chemical states of vanadium are quite similar to those in Ti, as shown in Fig. 8(c). The shares of oxidation states V(IV) in the DC film and V(IV) + V(V) in the unipolar pulsed DC film decrease rapidly to zero at 150 °C. The evolution behavior of the intermediate third valence state V(III) follows the same trend as for Ti(III), climbing up first at 150 °C and falling down when the annealing temperature is increased further. In the DC film, the oxidized vanadium has been reduced to its metallic state V^0 when the temperature is increased beyond 150 °C, however, such critical temperature is 160 °C for the unipolar pulsed DC film.

The situation is slightly different for the valence state evolution of Zr atoms. The share of predominant Zr(III) in the two as-received films

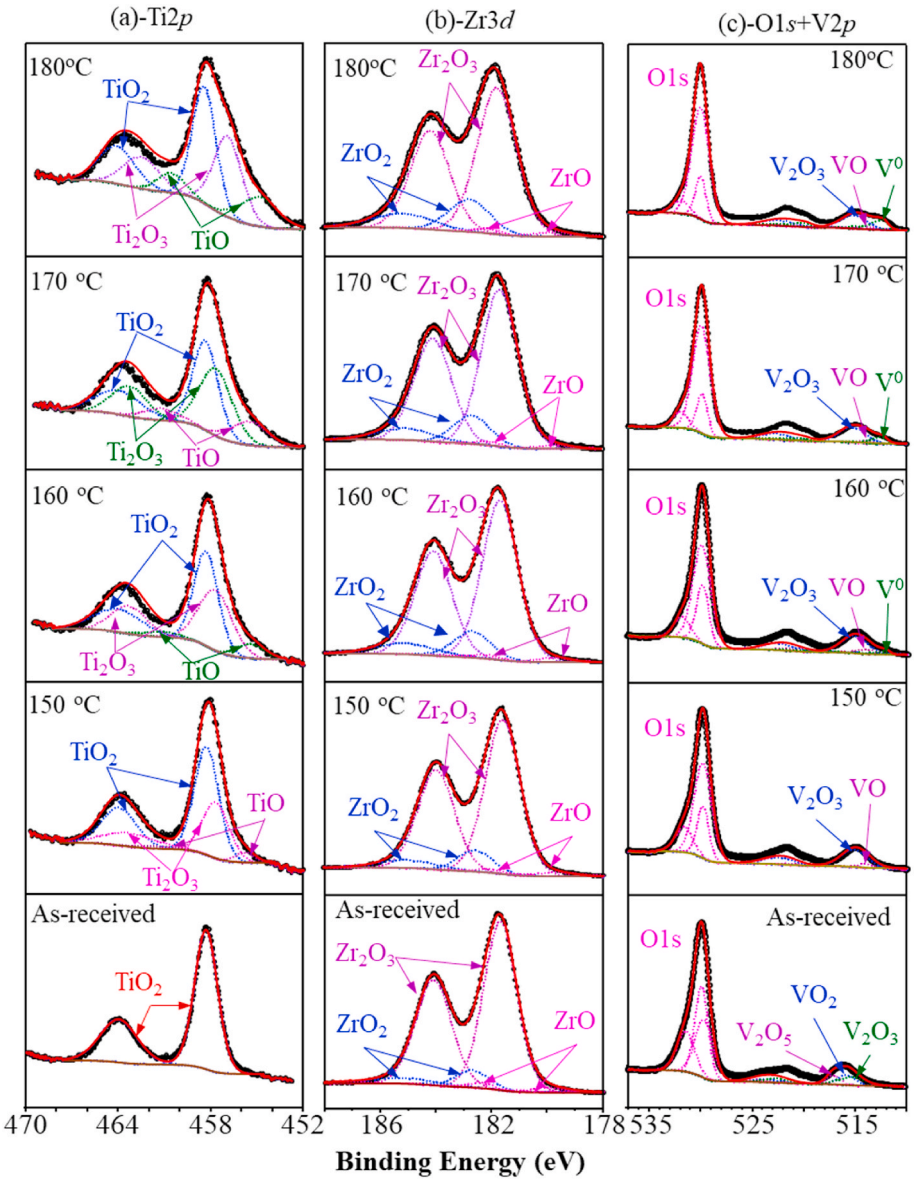

Fig. 7. Resolved XPS spectra collected from the unipolar pulsed DC film, (a) Ti 2p, (b) Zr 3d and (c) V 2p + O 1s orbitals. Discrete circles represent raw data, while the red line is the synthetic envelope. Dashed lines represent individual components resolved out of the collected spectra.

reduces gradually upon thermal treatment, which is accompanied by a slight increase in the fraction of Zr(IV). Oxidized Zr atoms have never been reduced to its metallic state Zr^0 in the two films. Though Zr(II) is observed in the DC film beyond 170 °C, its amount is very marginal. Based on the above consideration, it might be the case that Zr(III) is first oxidized to Zr(IV) upon heat treatment by capturing excessive oxygen atoms released by the reduction of titanium and/or vanadium oxides. It might be postulated that by further increasing the annealing temperature, the oxidized Zr atoms may also be reduced to their lower valence states and eventually to metallic Zr^0. The oxidation of Zr(III) to Zr(IV) might be dependent on the diffusion rate of oxygen towards the bulk of the film (such oxygen diffusion process is essential to restore the adsorption capacity of getter films), if the diffusion rate is fast enough, such oxidation may not take place (and it was not observed in our previous work [23]).

By comparing the valence state evolution of Ti, Zr and V atoms within the superficial regions of the two films (Fig. 8), two significant observations can be made. Firstly, during the annealing treatment, sequential reduction of Ti, Zr and V oxides is observed, with vanadium oxides being reduced the most easily, in agreement with existing literature [23,26,40,41]. It is also apparent that zirconium oxides are the hardest to be reduced in the Ti–Zr–V thin film; such behavior has also been reported in Ref. [39]. Secondarily, the share of metallic Ti^0 and V^0 in the DC film is much higher and their corresponding evolution rate against annealing temperature is faster than their counterparts in the unipolar pulsed DC film during thermal exposure. Such results indicate that the oxides within the DC film exhibit faster reduction kinetics than those in the unipolar pulsed DC film, which might be attributed to the higher surface roughness of the DC film as well as the higher grain boundary volumes arising from its much finer structure compared to that of the unipolar pulsed DC film (Fig. 1).

4. Conclusions

Ternary Ti–Zr–V getter films were deposited on OFC substrate under DC and unipolar pulsed DC current modes. Their microstructural characteristics were investigated. The evolution of chemical states with increasing annealing temperature in the superficial region of the films was quantitatively evaluated using X-ray photoelectron spectroscopy. The main findings are as follows:

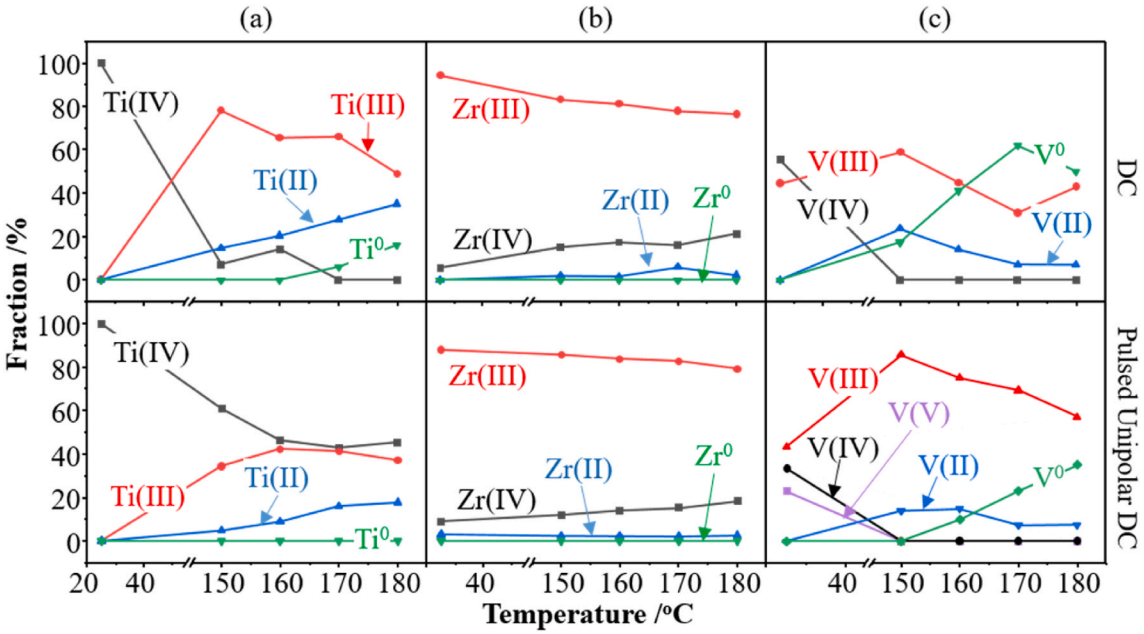

Fig. 8. Valence state evolution of (a) Ti, (b) Zr and (c) V with increasing annealing temperatures. The results for DC and unipolar pulsed DC films are presented in the first and second row respectively.

(1) Applied current mode induces significant effects on the morphologies of the thin films. While porous thin films were produced with both DC and unipolar pulsed DC current modes, DC current is beneficial to refine the microstructures, leading to slightly rougher surfaces, compared to the unipolar pulsed DC current.
(2) The native surface of the as-received film is covered by the oxides of Ti, Zr and V. During heating, sequential reduction of the initial oxides takes place, and V oxides are most easily to be reduced to metallic state V^0.
(3) The oxides within the DC thin film exhibit faster reduction kinetics as compared to those of the unipolar pulsed DC thin film.

Declaration of competing interest

The authors declare that they have no known competing financial interests or personal relationships that could have appeared to influence the work reported in this paper.

Acknowledgements

This work was supported by the National Natural Science Foundation of China (11905219), the Fundamental Research Funds for the Central Universities (WK2310000071) and the National Key Research and Development Program of China (2016YFA0402004).

References

[1] A. Gamelin, C. Bruni, D. Radevych, Longitudinal and transverse dynamics of ions from residual gas in an electron accelerator, Phys. Rev. Accelerator. Beams 21 (5) (2018), 054401.
[2] M. Brugger, H. Burkhardt, B. Goddard, F. Cerutti, R.G. Alia, Interactions of beams with surroundings, in: S. Myers, H. Schopper (Eds.), Particle Physics Reference Library : Volume 3: Accelerators and Colliders, Springer International Publishing, Cham, 2020, pp. 183–203.
[3] F. Broggi, A.R. Rossi, A. Bacci, L. Serafini, A. Cianchi, A. Clozza, G.D. Pirro, Effects of the Residual Gas Scattering in Plasma Acceleration Experiments and Linacs, PAC09, BC, Vancouver, 2009. Canada.
[4] R. Yang, T. Naito, S. Bai, A. Aryshev, K. Kubo, T. Okugi, N. Terunuma, D. Zhou, A. Faus-Golfe, V. Kubytskyi, S. Liu, S. Wallon, P. Bambade, Evaluation of beam halo from beam-gas scattering at the KEK Accelerator Test Facility, Phys. Rev. Accelerator. Beams 21 (5) (2018), 051001.
[5] P. He, Accelerator Vacuum Technology Challenges for Next Generation Synchrotron-Light Sources, IPAC2017, 2017. Copenhagen,Denmark.
[6] O.B. Malyshev, Non-evaporable Getter (NEG)-Coated Vacuum Chamber, Vacuum in Particle Accelerators: Modelling, Design and Operation of Beam Vacuum Systems, Wiley, 2020, pp. 175–213.
[7] A. Prodromides, Non-evaporable Getter Thin Film Coatings for Vacuum Applications, École Polytechnique, Lausanne, 2002.
[8] L. Lain Amador, Production of Ultra-high-vacuum Chambers with Integrated Getter Thin-Film Coatings by Electroforming, 2019.
[9] O.B. Malyshev, R. Valizadeh, A.N. Hannah, Pumping properties of Ti–Zr–Hf–V non-evaporable getter coating, Vacuum 100 (2014) 26–28.
[10] R. Širvinskaitė, O.B. Malyshev, R. Valizadeh, A. Hannah, M.D. Cropper, Single metal zirconium non-evaporable getter coating, Vacuum 179 (2020) 109510.
[11] M.C. Ruta Sirvinskaite, Adrian Hannah, Oleg Malyshev, Reza Valizadeh, Sihui Wang, Electron stimulated desorption from cryogenic NEG-coated surfaces, in: 10th International Particle Accelerator Conference, JACoW Publishing, Melbourne, Australia, 2019, p. TUPTS114.
[12] E.M. Bourim, H.Y. Kim, N.K. Chung, Development and characterization of non-evaporable getter thin films with Ru seeding layer for MEMS applications, Micromachines 9 (10) (2018).
[13] C. Benvenuti, P. Chiggiato, F. Cicoira, V. Ruzinov, Decreasing surface outgassing by thin film getter coatings, Vacuum 50 (1) (1998) 57–63.
[14] C. Benvenuti, P. Chiggiato, P. Costa Pinto, A. Escudeiro Santana, T. Hedley, A. Mongelluzzo, V. Ruzinov, I. Wevers, Vacuum properties of TiZrV non-evaporable getter films, Vacuum 60 (1) (2001) 57–65.
[15] V.V. Anashin, I.R. Collins, R.V. Dostovalov, N.V. Fedorov, A.A. Krasnov, O. B. Malyshev, V.L. Ruzinov, Comparative study of photodesorption from TiZrV coated and uncoated stainless steel vacuum chambers, Vacuum 75 (2) (2004) 155–159.
[16] R. Sharma, S. Bhattacharya, R. Tokas, K. Bhushan, S. Sen, S. Gadkari, S. Gupta, Deposition and in-situ characterization of Ti–Zr–V alloy thin films annealed at different temperatures under ultra-high vacuum conditions, J. Alloys Compd. 651 (2015) 375–381.
[17] M.P. Lozano, J. Fraxedas, XPS Analysis of the Activation Process in Non-evaporable Getter Thin Films, 30, 2000, pp. 623–627 (1).
[18] P. Chiggiato, P. Costa Pinto, Ti–Zr–V non-evaporable getter films: from development to large scale production for the Large Hadron Collider, Thin Solid Films 515 (2) (2006) 382–388.
[19] R. Valizadeh, O.B. Malyshev, J.S. Colligon, A. Hannah, V.M. Vishnyakov, Comparison of Ti-Zr-V nonevaporable getter films deposited using alloy or twisted wire sputter-targets, J. Vac. Sci. Technol. 28 (6) (2010) 1404–1412.
[20] L.-H. Wu, T.-C. Lin, C.-M. Cheng, C.-C. Chang, C.-K. Chan, S.-Y. Perng, I.C. Sheng, Comparative study of Ar-implanted Ti-Zr-V non-evaporable getter films on the Al-alloy substrate, AIP Adv. 8 (7) (2018), 075025.
[21] C. Benvenuti, P. Chiggiato, A. Mongelluzzo, A. Prodromides, V. Ruzinov, C. Scheuerlein, M. Taborelli, F. Lévy, Influence of the elemental composition and crystal structure on the vacuum properties of Ti–Zr–V nonevaporable getter films, J. Vac. Sci. Technol. 19 (6) (2001) 2925–2930.
[22] A.E. Prodromides, C. Scheuerlein, M. Taborelli, Lowering the activation temperature of TiZrV non-evaporable getter films, Vacuum 60 (1) (2001) 35–41.

[23] S. Wang, Z. Wang, X. Shu, W. Wei, Y. Gao, Y. Wang, Activation characterization of the Ti-Zr-V getter films deposited by magnetron sputtering, Appl. Surf. Sci. 528 (2020) 147059.
[24] C. Benvenuti, Pumping Device by Non-vaporisable Getter and Method for Using This Getter, 2002. United States.
[25] O.B. Malyshev, R. Valizadeh, J.S. Colligon, A. Hannah, K.J. Middleman, S. Patel, V. M. Vishnyakov, Influence of Deposition Pressure and Pulsed Dc Sputtering on Pumping Properties of Ti–Zr–V Nonevaporable Getter Films, 27, 2009, pp. 521–530 (3).
[26] C.-C. Li, J.-L. Huang, R.-J. Lin, C.-H. Chen, D.-F. Lii, Characterization of activated non-evaporable porous Ti and Ti–Zr–V getter films by synchrotron radiation photoemission spectroscopy, Thin Solid Films 515 (3) (2006) 1121–1125.
[27] J.A. Thornton, High Rate Thick Film Growth, vol. 7, 1977, pp. 239–260 (1).
[28] C. Benvenuti, P. Chiggiato, P.C. Pinto, A. Prodromides, V. Ruzinov, Influence of the substrate coating temperature on the vacuum properties of Ti–Zr–V non-evaporable getter films, Vacuum 71 (1) (2003) 307–315.
[29] P. Pokorný, J. Musil, P. Fitl, M. Novotný, J. Lančok, J. Bulíř, Contamination of magnetron sputtered metallic films by oxygen from residual atmosphere in deposition chamber, Plasma Process. Polym. 12 (5) (2015) 416–421.
[30] K. Wasa, M. Kitabatake, H. Adachi, 3 - sputtering phenomena, in: K. Wasa, M. Kitabatake, H. Adachi (Eds.), Thin Film Materials Technology, William Andrew Publishing, Norwich, NY, 2004, pp. 71–114.
[31] O.B. Malyshev, R. Valizadeh, R.M.A. Jones, A. Hannah, Effect of coating morphology on the electron stimulated desorption from Ti–Zr–Hf–V nonevaporable-getter-coated stainless steel, Vacuum 86 (12) (2012) 2035–2039.
[32] N. Gupta, Jagannath, R.K. Sharma, S.C. Gadkari, K.P. Muthe, R. Mukundhan, S. K. Gupta, Studies of thin films of Ti- Zr -V as non-evaporable getter films prepared by RF sputtering, AIP Con. Proc. 1512 (1) (2013) 794–795.
[33] G. Greczynski, L. Hultman, X-ray photoelectron spectroscopy: towards reliable binding energy referencing, Prog. Mater. Sci. 107 (2020) 100591.
[34] G. Greczynski, L. Hultman, C 1s peak of adventitious carbon aligns to the vacuum level: dire consequences for material's bonding assignment by photoelectron spectroscopy, ChemPhysChem 18 (12) (2017) 1507–1512.
[35] Y. Nakayama, H. Ishii, Exploration into the valence band structures of organic semiconductors by angle-resolved photoelectron spectroscopy, in: C.S.S.R. Kumar (Ed.), Surface Science Tools for Nanomaterials Characterization, Springer Berlin Heidelberg, Berlin, Heidelberg, 2015, pp. 367–404.
[36] J.F. Moulder, W.F. Stickle, P.E. Sobol, K.D. Bomben, Handbook of X-Ray Photoelectron Spectroscopy: A Reference Book of Standard Spectra for Identification and Interpretation of XPS Data, Perkin-Elmer Corporation, Minnesota, USA, 1992.
[37] L.L. Amador, P. Chiggiato, L.M.A. Ferreira, V. Nistor, A.T.P. Fontenla, M. Taborelli, W. Vollenberg, M.-L. Doche, J.-Y. Hihn, Development of copper electroformed vacuum chambers with integrated non-evaporable getter thin film coatings, J. Vac. Sci. Technol. 36 (2) (2018), 021601.
[38] M.C. Biesinger, L.W.M. Lau, A.R. Gerson, R.S.C. Smart, Resolving surface chemical states in XPS analysis of first row transition metals, oxides and hydroxides: Sc, Ti, V, Cu and Zn, Appl. Surf. Sci. 257 (3) (2010) 887–898.
[39] J. Zemek, P. Jiricek, XPS and He II photoelectron yield study of the activation process in Ti–Zr NEG films, Vacuum 71 (1) (2003) 329–333.
[40] J.H.E. Jeffes, Ellingham diagrams, in: K.H.J. Buschow, R.W. Cahn, M.C. Flemings, B. Ilschner, E.J. Kramer, S. Mahajan, P. Veyssière (Eds.), Encyclopedia of Materials: Science and Technology, Elsevier, Oxford, 2001, pp. 2751–2753.
[41] J. Kovac, O. Sakho, P. Manini, M. Sancrotti, Near-surface chemistry in Zr 2 Fe and ZrVFe studied by means of X-ray photoemission spectroscopy: a temperature-dependent study, J. Vac. Sci. Technol. Vac. Surfaces. Films. 18 (6) (2000) 2950–2956.